horticulturae

Article

Vegetation and Dormancy States Identification in Coniferous Plants Based on Hyperspectral Imaging Data

Pavel A. Dmitriev *, Boris L. Kozlovsky and Anastasiya A. Dmitrieva

Botanical Garden, Academy of Biology and Biotechnologies, Southern Federal University, Rostov-on-Don 344006, Russia; blk@sfedu.ru (B.L.K.); admit@sfedu.ru (A.A.D.)
* Correspondence: pdmitriev@sfedu.ru

Abstract: Conifers are a common type of plant used in ornamental horticulture. The prompt diagnosis of the phenological state of coniferous plants using remote sensing is crucial for forecasting the consequences of extreme weather events. This is the first study to identify the "Vegetation" and "Dormancy" states in coniferous plants by analyzing their annual time series of spectral characteristics. The study analyzed *Platycladus orientalis*, *Thuja occidentalis* and *T. plicata* using time series values of 81 vegetation indices and 125 spectral bands. Linear discriminant analysis (LDA) was used to identify "Vegetation" and "Dormancy" states. The model contained three to four independent variables and achieved a high level of correctness (92.3 to 96.1%) and test accuracy (92.1 to 96.0%). The LDA model assigns the highest weight to vegetation indices that are sensitive to photosynthetic pigments, such as the photochemical reflectance index (PRI), normalized PRI (PRI_norm), the ratio of PRI to coloration index 2 (PRI/CI2), and derivative index 2 (D2). The random forest method also diagnoses the "Vegetation" and "Dormancy" states with high accuracy (97.3%). The vegetation indices chlorophyll/carotenoid index (CCI), PRI, PRI_norm and PRI/CI2 contribute the most to the mean decrease accuracy and mean decrease Gini. Diagnosing the phenological state of conifers throughout the annual cycle will allow for the effective planning of management measures in conifer plantations.

Keywords: vegetation indices; photochemical reflectance index; *Platycladus orientalis*; acclimatization; deacclimatization

Citation: Dmitriev, P.A.; Kozlovsky, B.L.; Dmitrieva, A.A. Vegetation and Dormancy States Identification in Coniferous Plants Based on Hyperspectral Imaging Data. *Horticulturae* **2024**, *10*, 241. https://doi.org/10.3390/horticulturae10030241

Academic Editors: Zhouli Liu and Yi Zhao

Received: 9 February 2024
Revised: 26 February 2024
Accepted: 29 February 2024
Published: 1 March 2024

1. Introduction

A precise and objective evaluation of the condition of woody plants during their annual development cycle is crucial for anticipating the effects of exposure to extreme temperatures, including untimely negative and positive temperatures. This task is especially relevant in the context of climate change, where the winter temperature regime has become increasingly unstable [1,2]. Winter temperature fluctuations significantly affect the cultivation of woody ornamental plants [3].

The annual cycle of the development of woody plants in the temperate climate zone consists of two main stages: vegetation and dormancy. The transition from vegetation to dormancy is carried out via acclimatization, and the reverse process is carried out by deacclimatization. Plants undergo complex morphological, physiological, biochemical, and genetic changes during these processes [4–7]. Coniferous plants undergo changes in the structure of their photosynthetic apparatus, as well as during photoinhibition and other related processes [8–10]. Significant differences in the state of the photosynthetic apparatus of coniferous plants during the periods of vegetation and dormancy are a prerequisite for the identification of these states via spectral reflections using remote sensing.

Acclimatization is a two-step process [11]. The first stage of this process is cold acclimation, which is initiated by short daylight hours and proceeds at low positive temperatures. This stage leads to the emergence of plant resistance to cold and frost. The second phase of acclimatization, which involves gaining cold hardiness, occurs at negative temperatures that do not freeze plants. This process enables a particular species to achieve its maximum frost resistance. This is a period of deep dormancy (endo-dormancy) during which the plant's growth cannot resume even under favorable conditions. In the latter half of winter, deep dormancy transitions into a state of forced dormancy (eco-dormancy), during which the plant's growth is only restrained by unfavorable weather conditions.

The process of transition from the state of eco-dormancy to the state of vegetation (deacclimatization) in plants has been studied less than the process of acclimatization [1]. This process occurs at the end of winter or in spring under the influence of positive temperatures. After deacclimatization, the plants resume vegetation.

The completion of the processes of acclimatization and deacclimatization is not manifested in external signs; therefore, it cannot be established via phenological methods. For example, the phenological phases of "bud break" and "beginning of shoot growth", which are taken as the beginning of the plant's vegetation, occur later than the completion of the deacclimatization process [12–14]. Therefore, in accordance with phenological characteristics, a plant that is at rest may already be vulnerable to recurrent frosts. According to phenological characteristics, it is also impossible to determine that the plant has passed the second stage of acclimatization (gaining cold hardiness) and has reached maximum frost resistance.

An objective assessment of the frost resistance of woody plants can be obtained via the methods of electrolyte leakage, chlorophyll fluorometry, differential thermal analysis, electrical impedance spectroscopy, and others [15,16]. However, these methods of diagnosing frost resistance are quite laborious and slow. Therefore, it is necessary to develop prompt and relatively simple methods for assessing frost resistance, as well as diagnosing the states of vegetation and dormancy of plants. Such contact methods include an analysis of the amplitude–kinetic characteristics of chlorophyll fluorescence [17,18]. The development of technology for monitoring the solar-induced fluorescence (SIF) of chlorophyll using satellites is currently only at the stage of exploratory research [19,20]. Passive methods of remote sensing have been developed to a much greater extent. Using spectral sensors, it is possible to remotely diagnose the physiological and biochemical characteristics of plants—the content of chlorophylls [21], macroelements [22–25], water [26,27], and nitrogen [28,29]. Spectral sensors proved to be effective in diagnosing stress in plants under the influence of high [30–34] and low temperatures [35].

Vegetation indices (VIs) are utilized to describe plant phenology through remote sensing. Other metrics, such as the leaf area index (LAI) [36] and maximum quantum yield of photosystem II (PSII) [37], are used less frequently. Among the VIs, the normalized difference vegetation index (NDVI) and the extended vegetation index (EVI) [38–41] are the most commonly used.

Whereas the phenology of deciduous plants can be described fairly accurately via a time series of chlorophyll-sensitive VIs, tracking the phenology of evergreens is much more difficult because they retain leaves and photosynthetic pigments throughout the year. At the same time, the LAI of conifers varies little with season [42]. The content of photosynthetic pigments, especially xanthophyll cycle pigments, changes to a greater extent. Therefore, the "photosynthetic phenology" of conifers is well described by the photochemical reflectance index (PRI) and chlorophyll/carotenoid index (CCI), which are related to the carotenoid content and the proportion of chlorophylls and carotenoids [37,43–46].

Further accumulation of factual material on a wide range of species, climatic conditions, and VIs is required for the development of remote sensing phenology of evergreen plants. The possibility of diagnosing "Vegetation" and "Dormancy" states of conifers using remote sensing remains an open question.

Objectives of the study: to correlate spectral responses and climatic adaptations of species of the genus Thuja and Platycladus and to develop hyperspectral remote sensing tools to assess species adaptations to climatic stress.

2. Conditions, Objects, and Methods

2.1. Study Region

The study was conducted at the Botanical Garden of Southern Federal University in Rostov-on-Don, Russia (47°13′ N; 39°39′ E). The study utilized plant specimens from the collection of holosemal plants at the Botanical Garden.

2.2. Meteorological Characteristics

Rostov-on-Don has a moderately continental and arid climate, with moderately mild winters and hot summers (Climate of Rostov-on-Don, 1987). The average annual air temperature is +8.9 °C, with an average temperature of −5.7 °C in January and +23 °C in July. The average annual rainfall is 548 mm.

The growing season in 2022 (the period from the transition of the average daily air temperature above +5 °C to the decrease in the average daily air temperature below +5 °C) began on 29 March and ended on 1 November. In 2023, the growing season began on 1 April.

The periods of acclimatization and deacclimatization were determined by indirect indicators, such as the length of the day and the daily temperature fluctuations.

Figure 1 presents the seasonal dynamics of daily air temperatures from 22 January 2022 to 23 May 2023.

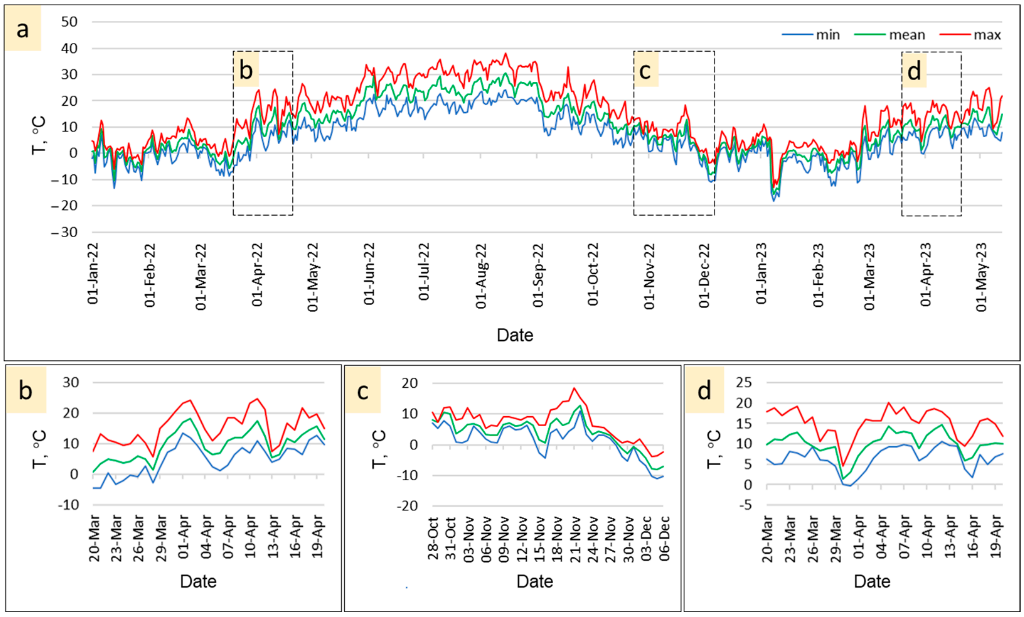

Figure 1. Seasonal dynamics of air temperature. (**a**): The entire study period. (**b**): Deacclimatization period in spring 2022. (**c**): Acclimatization period in autumn 2022. (**d**): Deacclimatization period in spring 2023. Min—minimum temperature per day; mean—average temperature per day; max—maximum temperature per day.

Deacclimatization period in spring 2022. Daylight hours began to exceed 12 h after 18 March. On 29 March, the minimum daily air temperature steadily exceeded 0 °C (further on, the minimum daily temperature did not fall below 0 °C, which excludes the reacclimatization process), and on 15 April, the average daily temperature steadily exceeded +10 °C.

Acclimatization period in autumn 2022. Daylight hours began to be less than 12 h after 25 September. The average daily temperature dropped below +10 °C since 1 November. The first nighttime negative temperatures (−2.7 °C) were recorded on 30 November. A sharp decrease in the average daily temperature to −8.0 °C occurred on 4 December and lasted for 4 days. Such a temperature regime is lethal for non-acclimatized woody plants. Therefore, it is believed that the acclimatization of woody plants occurred between 1 November and 30 November 2022. By 4 December, the plants had already entered dormancy.

Deacclimatization period in spring 2023. On 24 March, the minimum daily air temperature steadily exceeded 0 °C (further on, the minimum daily temperature did not fall below 0 °C, which excludes the reacclimatization process), and on 17 April, the average daily temperature steadily exceeded +5 °C.

According to the periods of acclimatization and deacclimatization, the following time frames for the dormancy and vegetation of experimental coniferous plants were established:

— Winter dormancy for 2021–2022 ended on 29 March 2022.
— Vegetation started on 15 April 2022 and ended on 1 November 2022.
— The plants entered dormancy on 30 November 2022 and left it on 24 March 2023.
— Vegetation started again on 17 April 2023.

2.3. Objects of Study

Three plant species from the genera Thuja and Platycladus were the objects of the study.

Thuja occidentalis L.—evergreen tree 12–20 m high. The natural range is located in the southeastern part of Canada and the northern part of the United States. This plant is highly frost-resistant—USDA (United States Department of Agriculture) hardiness zone 6a. *T. occidentalis* is a hygrophilous plant. Within its natural range, it has a positive growth response to humidity conditions and a neutral response to temperature [47]. In the study area, *T. occidentalis* suffers from drought and high summer temperatures [48].

T. plicata Donn ex D. Don—tall (up to 60 m) evergreen tree. The natural range of the species is located in the northwest of North America. Ecologically, *T. plicata* is similar to *T. occidentalis*. USDA zone—6b.

Platycladus orientalis (L.) Franco—evergreen low (up to 12 m) tree. The natural range is in China and locally in South Korea. The plant is highly drought tolerant and heat tolerant. The frost tolerance of this tree is not as high as *T. occidentalis* (USDA frost tolerance zone—7a). Thermal factors play a more important role in *P. orientalis* culture expansion than humidity factors [49].

Thus, at the study site, the critical season in the annual development cycle for *P. orientalis* is winter, and for *T. occidentalis* and *T. plicata*, summer.

Each species was represented in the experiment by three specimens. All plant samples grew under the same conditions. Seven shoots were taken from each plant sample and transported to the laboratory within an hour. The shoots contained first and second year growths.

2.4. Hyperspectral Imaging Technique

The study presented here used a time series of 81 VIs and 125 spectral bands (SBs) to cover two periods of deacclimatisation, one period of acclimatisation, and one period of vegetation and dormancy of three coniferous plant species: *Thuja occidentalis*, *T. plicata*, and *Platycladus orientalis*. The most informative VIs and SB for describing the phenological cycle of coniferous plants were determined, and their "Vegetation" and "Dormancy" states were identified.

Hyperspectral imaging (HSI) was carried out in laboratory conditions with an interval of 7–10 days from 2 February 2022 to 10 May 2023. There were 57 HSI in total.

For HSI, a Cubert UHD-185 hyperspectral camera (Cubert GmbH, Ulm, Germany) was used [50,51]. Hyperspectral imaging was conducted using artificial illuminants that had a spectral range overlapping with that of the hyperspectral camera. During the HSI, the camera lens was positioned at 40 cm from the object and directed perpendicular to it. Plant shoots were stacked (Figure 2a). Before each HSI, the shoots in the stack were moved from bottom to top. Seven HSI were made for each stack.

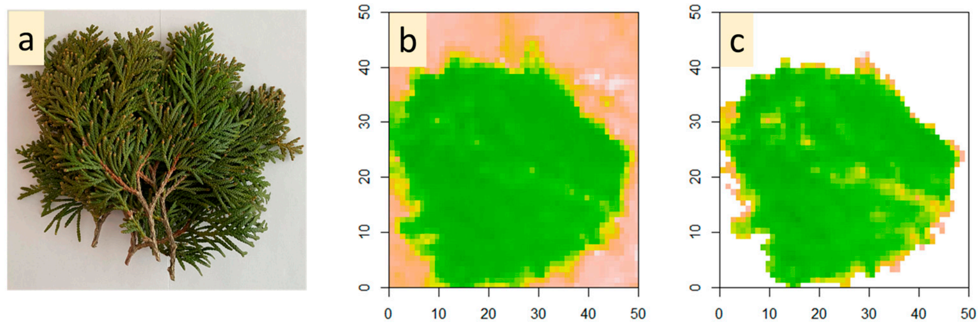

Figure 2. Selection ROI. Stack of shoots of *T. occidentalis* (**a**), hyperspectral image before (**b**) and after (**c**) threshold setting "Carter5 > 1.4".

2.5. Hyperspectral Imagery Data Preprocessing

During the preprocessing stage, noise was removed from the spectra by using a Savitsky–Golay filter with a length of 15 nm. To select the region of interest (ROI), the threshold of the vegetation index (VI) Carter5 was used with a value of more than 1.4 [52] (Figure 2b,c).

The selection of spectral profiles (pixels) from the image was achieved through automated repeated random selection.

2.6. Calculation of Vegetation Indices

Hyperspectral imaging data were used to calculate PRI, CCI, and NDVI for plant phenology analysis. It should be noted that these VIs have traditionally been used to describe plant growth and development. The formulas for calculating these VIs are provided below [45,53,54].

$$\mathrm{NDVI} = \frac{\mathrm{R}_{900} - \mathrm{R}_{680}}{\mathrm{R}_{900} + \mathrm{R}_{680}}$$

$$\mathrm{PRI} = \frac{\mathrm{R}_{528} - \mathrm{R}_{570}}{\mathrm{R}_{528} + \mathrm{R}_{570}}$$

$$\mathrm{CCI} = \frac{\mathrm{R}_{528} - \mathrm{R}_{645}}{\mathrm{R}_{528} + \mathrm{R}_{645}}$$

where R_{xxx}: reflectance at the wavelength "xxx".

Additionally, 78 more VIs were calculated. Details regarding these VIs can be found in Dmitriev et al. [55].

2.7. Hyperspectral Imagery Data Processing

The study employed the non-parametric Spearman correlation coefficient to identify the most informative VIs for describing conifer phenology. To identify the "Vegetation" and "Dormancy" states of conifers, linear discriminant analysis (LDA) and random forest (RF) were used. The statistical calculations were performed using the R environment (R Core Team, Vienna, Austria).

3. Results

3.1. Correlation Analysis between Spectral and Climate Data

The processes of acclimatization and deacclimatization and the state of plants during vegetation and dormancy are closely related to temperature and daylight hours. The dynamics of daily temperature allows us to indirectly divide the "Vegetation" and "Dormancy" periods in the annual development cycle of woody plants. Therefore, an assessment was made of the closeness of the relationship between the values of VIs, SB, and the average daily temperature, as well as the duration of daylight hours. For this, the nonparametric Spearman correlation coefficient (r) was used. In the annual cycle of plant development, only 4 out of 81 VIs had a high correlation strength with the average daily temperature

($r > 0.7$ according to the Chaddock scale) simultaneously for *P. orientalis*, *T. occidentalis*, and *T. plicata* (Table 1). These were CCI, PRI, ratio of PRI to coloration index 2 (PRI/CI2), and normalized PRI (PRI_norm). These VIs also had a high and statistically significant correlation with daylight hours.

Table 1. The value of the Spearman correlation coefficient between the values of VI and the average daily temperature, as well as between the values of VI and the length of daylight hours in the annual cycle of plant development.

P. orientalis			***T. occidentalis***			***T. plicata***		
VI	***r***	***p*-Value**	**VI**	***r***	***p*-Value**	**VI**	***r***	***p*-Value**
Average daily temperature, °C								
PRI_norm	−0.8	0.001	PRI/CI2	0.85	0.001	PRI/CI2	0.83	0.001
PRI	0.84	0.001	PRI	0.84	0.001	PRI	0.81	0.001
PRI/CI2	0.82	0.001	PRI_norm	−0.8	0.001	PRI_norm	−0.8	0.001
CCI	0.8	0.001	CCI	0.77	0.001	CCI	0.72	0.001
DPI	0.79	0.001	DPI	0.72	0.001	DPI	0.65	0.001
Vogelmann3	0.76	0.001	RARS	−0.6	0.001	RARS	−0.6	0.001
D2	−0.8	0.001	CRI2	−0.6	0.001	CRI2	−0.6	0.001
MTCI	0.72	0.001	CRI1	−0.6	0.001	CRI1	−0.6	0.001
D1	0.72	0.001	Gitelson2	0.56	0.001	Gitelson2	0.51	0.001
NDVI	0.28	0.03	NDVI	0.09	0.50	NDVI	0.07	0.58
Day length, day								
CCI	0.78	0.001	PRI	0.75	0.001	PRI_norm	−0.7	0.001
PRI_norm	−0.7	0.001	PRI/CI2	0.73	0.001	PRI/CI2	0.65	0.001
PRI	0.72	0.001	PRI_norm	−0.7	0.001	CCI	0.65	0.001
PRI/CI2	0.71	0.001	CCI	0.69	0.001	PRI	0.65	0.001
DWSI4	0.7	0.001	DPI	0.64	0.001	RARS	−0.6	0.001
NDVI3	−0.7	0.001	D1	0.56	0.001	CRI2	−0.5	0.001
GI	0.69	0.001	Vogelmann2	−0.5	0.001	DPI	0.52	0.001
Datt5	−0.7	0.001	Vogelmann4	−0.5	0.001	Gitelson2	0.47	0.001
GMI1	−0.6	0.001	D2	−0.5	0.001	CRI1	−0.5	0.001
NDVI	0.31	0.02	NDVI	0.24	0.08	NDVI	0.2	0.14

Note: VI—vegetation index. *r*—correlation coefficient. *p*-value—level of significance.

The time series of the CCI, double peak index (DPI), PRI, PRI/CI2, and PRI_norm values, in contrast to NDVI, have a well-defined seasonal character (Figure 3).

Preliminarily, it can be stated that the "Dormancy" state of experimental evergreens is characterized by the following VIs values: CCI < 0.15; DPI < 0.075; PRI < −0.05; PRI/CI2 < −0.04; and PRI_norm > 0.003.

The strength of association of the SB with the mean daily temperature and day length is much lower than that of VIs. The highest value of the correlation coefficient ($0.42 < r < 0.57$, at $p < 0.001$) with the average daily temperature has an SB in the range from 514 to 542 nm (Table 2).

3.2. Linear Discriminant Analysis of States "Dormancy" and "Vegetation"

In accordance with the periods of "Vegetation" and "Dormancy" identified by climatic characteristics, the HSI data were divided into two classes. "Vegetation" class—HSI data obtained in the interval from 15 April 2022 to 1 November 2022. "Dormancy" class—HSI data obtained in the interval from 30 November 2022 to 24 March 2023.

Each class was divided into two subsets: 70% (training set) spectral data for model building and the remaining 30% (test set) spectral data used for validation. The LDA for

81 Vis gave good results. The testing accuracy for *P. orientalis*, *T. occidentalis*, and *T. plicata* was 99.8, 96.9, and 96.0%, respectively (Figure 4a,b).

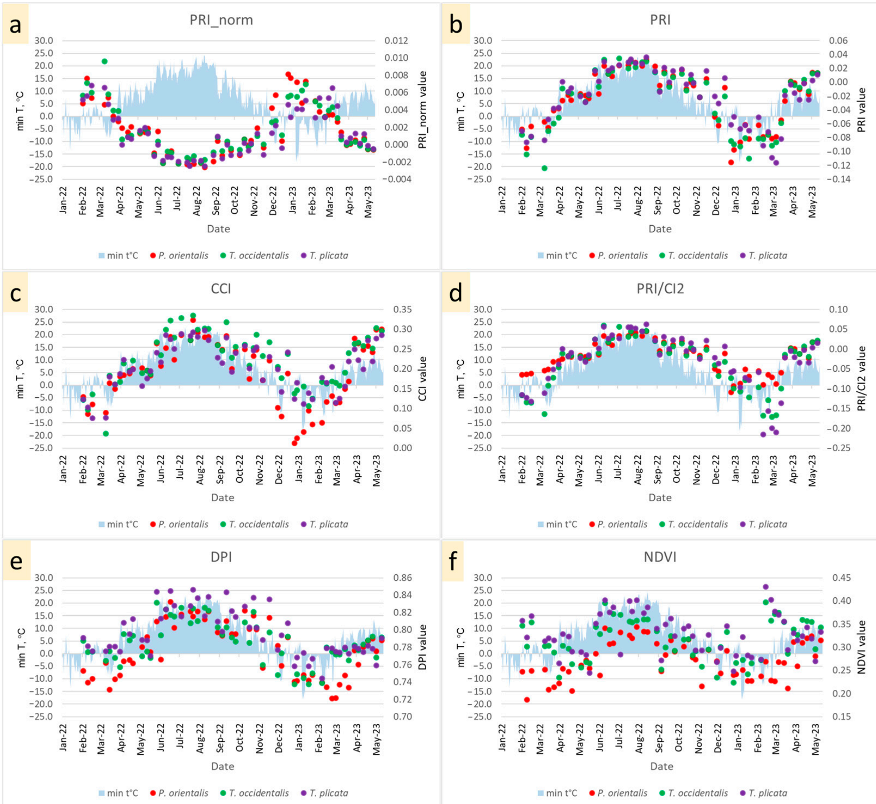

Figure 3. Seasonal dynamics of PRI_norm (**a**), PRI (**b**), CCI (**c**), PRI/CI2 (**d**), DPI (**e**), and NDVI (**f**) values compared to the dynamics of the daily temperature.

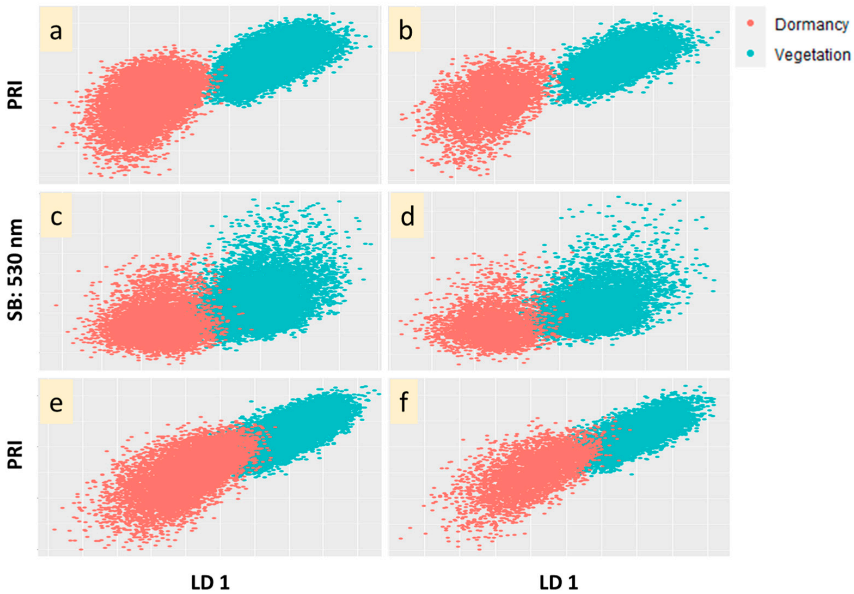

Figure 4. Linear discriminant analysis of two states of *P. orientalis*: "Vegetation" and "Dormancy". (**a**): Using 81 VIs (training set); (**b**): using 81 VIs (test set); (**c**): using 125 SB (training set); (**d**): using 125 SB (test set); (**e**): using LDA model LD1 = 0.82 PRI − 0.73 PRI_norm − 0.82 D2 (training set); (**f**) using LDA model LD1 = 0.82 PRI − 0.73 PRI_norm − 0.82 D2 (test set).

A similar result was obtained for 125 SB (Figure 4c,d). The testing accuracy for *P. orientalis*, *T. occidentalis*, and *T. plicata* was 97.7, 92.9, and 92.5, respectively.

The stepwise classification results, using a 10-fold cross-validated correctness rate of the method LDA, provided that adding the next factor does not increase the accuracy by more than 1%, are presented in Table 3.

Table 2. The value of the Spearman correlation coefficient between the values of the SB and the average daily temperature and daylight hours in the annual cycle of plant development.

P. orientalis			*T. occidentalis*			*T. plicata*		
SB	***r***	***p*-Value**	**SB**	***r***	***p*-Value**	**SB**	***r***	***p*-Value**
Average daily temperature, °C								
518	0.46	0.001	526	0.57	0.001	526	0.46	0.001
522	0.45	0.001	530	0.57	0.001	522	0.45	0.001
526	0.45	0.001	522	0.56	0.001	530	0.44	0.001
514	0.44	0.001	534	0.55	0.001	518	0.43	0.001
530	0.43	0.001	518	0.54	0.001	534	0.42	0.001
698	−0.43	0.001	538	0.53	0.001	514	0.39	0.001
694	−0.43	0.001	514	0.51	0.001	538	0.38	0.001
690	−0.42	0.001	542	0.51	0.001	510	0.36	0.010
534	0.42	0.001	510	0.47	0.001	542	0.36	0.010
702	−0.42	0.001	546	0.47	0.001	546	0.32	0.020
Day length, day								
526	0.44	0.001	526	0.44	0.001	526	0.45	0.001
530	0.44	0.001	522	0.44	0.001	522	0.45	0.001
534	0.44	0.001	530	0.44	0.001	530	0.45	0.001
538	0.43	0.001	518	0.43	0.001	534	0.44	0.001
522	0.43	0.001	534	0.41	0.001	518	0.43	0.001
518	0.43	0.001	514	0.41	0.001	514	0.40	0.001
542	0.42	0.001	538	0.39	0.001	538	0.40	0.001
546	0.41	0.001	510	0.38	0.001	926	0.38	0.001
514	0.41	0.001	918	0.38	0.001	542	0.38	0.001
550	0.40	0.001	922	0.37	0.010	922	0.38	0.001

Note: SB—spectral band. *r*—correlation coefficient. *p*-value—level of significance.

All LDA models have high model correctness rates and testing accuracy (Table 3, Figure 4e,f).

It should be noted that the LDA models based on the SBs have lower values of the model correctness rate and testing accuracy than the LDA models based on the VIs (Table 3). To improve the accuracy of testing the LDA model based on the SBs, it will be necessary to use many SBs, which contribute little to the accuracy of the model. From a practical point of view, this is a problem since remote sensing will have to use expensive multichannel spectral sensors. Thus, the use of VIs to identify the states of "Vegetation" and "Dormancy" of evergreens gives better results than the use of SBs. The basis of LDA models is the indices of the "PRI group".

3.3. Random Forest Pixel-Based Testing of States "Dormancy" and "Vegetation"

RF pixel-based test was used to identify the states of "Vegetation" and "Dormancy" in experimental plants.

The following dataset was used for the training set (Figure 5): "Vegetation" class—HSI data obtained in the interval from 15 April 2022 to 1 November 2022. "Dormancy" class—HSI data obtained in the interval from 30 November 2022 to 24 March 2023.

Table 3. LDA models for the two target classes "Vegetation" and "Dormancy".

Species	Final Model	Model Correctness Rate, %	Testing Accuracy, %
	VIs		
P. orientalis	LD1 = 0.82 PRI − 0.73 PRI_norm − 0.82 D2	97.20	97.01
T. occidentalis	LD1 = 0.77 PRI − 0.72 PRI_norm + 0.57 PRI/CI2	94.45	93.97
T. plicata	LD1 = 0.68 PRI − 0.53 PRI_norm + 0.43 PRI/CI2 + 0.39 D1	92.31	92.10
All species	LD1 = 0.75 PRI − 0.69 PRI_norm + 4.44 PRI/CI2 − 0.44 D2	96.09	96.03
	SB		
P. orientalis	LD1 = $-0.65\ R_{450} + 0.37\ R_{522} + 0.37\ R_{526} + 0.38\ R_{530} + 0.37\ R_{534} - 0.39\ R_{686}$	88.63	88.14
T. occidentalis	LD1 = $-0.52\ R_{450} + 0.38\ R_{518} + 0.41\ R_{522} + 0.40\ R_{526} + 0.37\ R_{530}$	87.40	87.67
T. plicata	LD1 = $-0.63\ R_{450} + 0.31\ R_{522} + 0.32\ R_{526} + 0.31\ R_{530} + 0.36\ R_{906} + 0.34\ R_{910}$	83.72	83.79
All species	LD1 = $R_{450} + R_{518} + R_{522} + R_{526} + R_{530}$	86.56	87.56

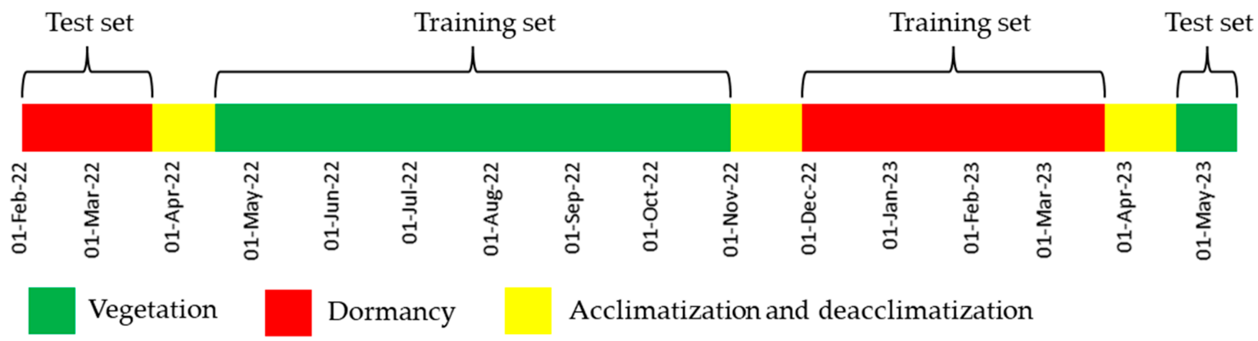

Figure 5. Classes for dataset in random forest classification.

For the test set, the HSI data were also divided into two classes (Figure 5): "Vegetation" class—HSI data obtained in the following calendar dates: 19 April, 26 April, 2 May, and 10 May 2023. "Dormancy" class—HSI data obtained in the interval from 2 February to 23 March 2022.

The RF used number of trees 100 (Figure 6), the number of variables tried at each split: 8. The confusion matrix obtained from the RF pixel-based classification of 81 VIs for the two target classes "Vegetation" and "Dormancy" for *P. orientalis* is presented in Table 4. The out-of-bag (OOB) estimate of the error rate was only 0.16%.

Table 4. Confusion matrix obtained from the RF pixel-based classification of 81 VIs for two target classes "Vegetation" and "Dormancy" for *P. orientalis*.

State	Dormancy	Vegetation	Error, %
	Training set		
Dormancy	11,966	34	0.28
Vegetation	27	22,973	0.12
	Test set		
Dormancy	6000	0	0
Vegetation	274	3726	6.85

The largest contributors to the mean decrease accuracy and mean decrease Gini values are CCI, PRI, and PRI_norm (Figure 7).

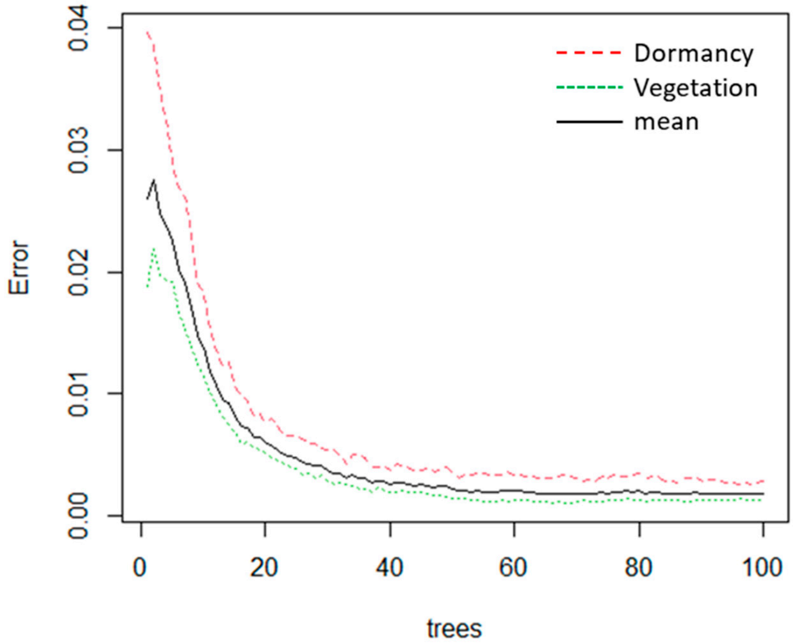

Figure 6. Effect of the number of trees on OOB error rate estimation for RF classification of "Vegetation" and "Dormancy" states.

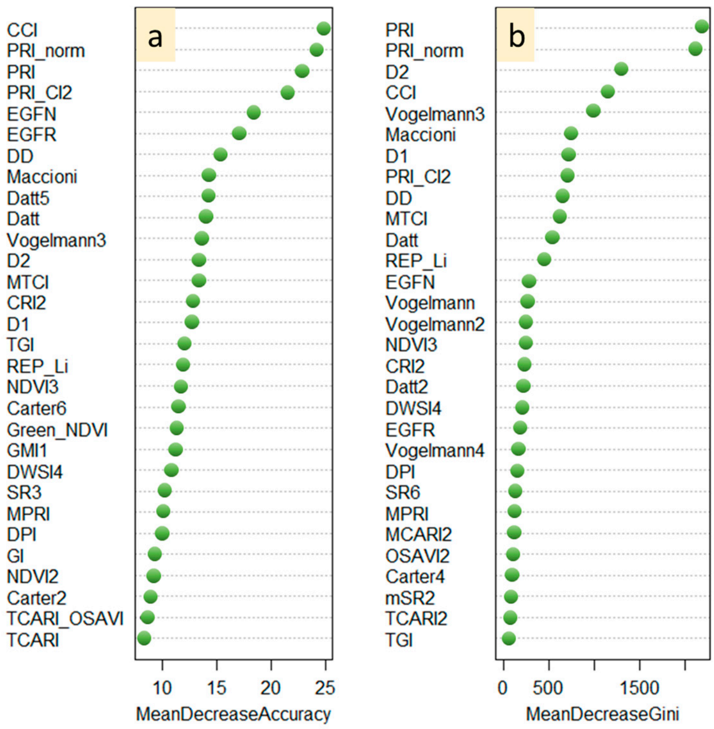

Figure 7. Ranking of importance of VIs for differences between the two target classes "Vegetation" and "Dormancy". Vegetation indices are ranked from top to bottom from the most important to the least important by contribution to mean decrease accuracy (**a**) and mean decrease Gini (**b**).

The overall testing accuracy was 97.26%. The "Dormancy" state was tested without error, and the "Vegetation" state was tested with an error of 6.85% (Table 4).

According to the same scheme, RF testing was carried out using the most informative VIs (PRI, PRI_norm, PRI/CI2, and D2) selected based on the results of the LDA (Table 5).

Table 5. Confusion matrix obtained from the RF pixel-based classification of four VIs (PRI, PRI_norm, PRI/CI2, and D2) for two target classes "Vegetation" and "Dormancy" for *P. orientalis*.

State	Dormancy	Vegetation	Error, %
Training set			
Dormancy	11,637	363	3.03
Vegetation	368	22,632	1.60
Test set			
Dormancy	5873	127	2.12
Vegetation	212	3788	5.30

The error of testing the state "Dormancy" was 2.12%, and the error of testing the state "Vegetation" was 5.30%. Thus, the number of VIs for identifying the states of vegetation and dormancy in conifers can be significantly reduced. Similar RF test results are also obtained for *T. occidentalis* and *T. plicata*.

4. Discussion

The photosynthetic phenology of plants reflects the seasonal variation in photosynthetic activity, pigment concentrations, and the ratio of their pools using VIs time series and spectral channels [56–58]. Unlike classical phenology, photosynthetic phenology can describe the complete annual development cycle of coniferous plants. It can record both qualitative and quantitative changes in plant states and determine the rate of plant development and senescence [39,59]. Additionally, photosynthetic phenology provides crucial parameters for gross primary productivity models [58]. The PRI and CCI indices, which are sensitive to carotenoids, show potential as metrics for the phenological process in conifers [37,43–46,60]. The use of photosynthetic phenology methods to identify the "Vegetation" and "Dormancy" states in coniferous plants, as well as the transitions between these states (acclimatization and deacclimatization), is of great scientific and practical interest. This study is the first to identify vegetation and winter dormancy states in conifers by analyzing their annual time series of SBs and VIs. The classification was performed using machine learning methods, which are commonly used to predict photosynthetic pigment content [61,62]. The study found that VIs were better metrics for describing annual dynamics in *T. occidentalis*, *T. plicata*, and *P. orientalis* and diagnosing "Vegetation" and "Dormancy" states than SBs.

The correlation analysis revealed that 4 out of 81 vegetation indices (CCI, PRI, PRI/CI2, and PRI_norm) have a strong relationship ($r > 0.7$) with both annual temperature dynamics and daylight hours for all investigated coniferous species. Another group of vegetation indices (CRI1, CRI2, D2, Datt5, DPI, GMI, Gitelson2, RARS, Vogelman, etc.) showed a moderate association ($0.5 < r < 0.7$) with meteorological characteristics. The statistical analysis revealed that there was no significant correlation between NDVI values and meteorological characteristics. Additionally, spectral bands showed a weaker correlation with these meteorological characteristics. The LDA models used to identify the "Vegetation" and "Dormancy" states of *P. orientalis* by VIs contained three to four independent variables, resulting in a high degree of model correctness (ranging from 92.31% to 96.09%) and high test accuracy (ranging from 92.10% to 96.03%). The LDA model identified PRI, PRI_norm, PRI/CI2, and D2 as having the highest weight. The accuracy of LDA models for spectral channels was below 90%. The RF method can identify "Vegetation" and "Dormancy" states with high accuracy. For *P. orientalis*, 81 VIs had a testing accuracy of 97.26%. The most significant contributors to mean decrease accuracy and mean decrease Gini values are CCI, PRI, PRI_norm, and PRI/CI2.

Thus, four carotenoid-sensitive Vis–PRI, PRI_norm, PRI/CI2, and CCI were found to be the most effective in classifying phenological states of experimental plants. The vegetative index PRI is sensitive to rapid changes (within a day) in the state of de-epoxidation, which is a signal of the mutual transformation of xanthophylls. This vegetative index can also be used to track long-term changes in the ratio of chlorophyll and carotenoid pools [45,54,63–66]. PRI indirectly reflects the water content of vegetation [67–70]. Moreover, PRI is an effective tool for diagnosing plant stress [43,71–74]. This effectiveness can be attributed to the fact that the ratio of chlorophyll and carotenoid pools serves as an indicator of the seasonal regulation of photosynthesis and gross primary productivity [75]. During the transition from vegetation to dormancy in coniferous plants, there is a change in the proportions of photosynthetic pigments and the structure of the photosynthetic apparatus. Additionally, there is a steady decrease in the efficiency of PSII [9,10]. For instance, in common pine, the winter suppression of photosynthesis is accompanied by a loss of chlorophylls and a twofold increase in xanthophyll cycle pigments due to light stress [8]. During the transition to winter dormancy, woody plants experience a decrease in tissue water content [76]. The seasonal dynamics of conifers are well described by PRI. However, PRI has a disadvantage of being highly sensitive to light level [77]. On the other hand, CCI records only stable long-term changes in pigments and responds synchronously to seasonal changes in chlorophyll and carotenoid ratios as well as photosynthetic activity [37,45]. It is important to note that the CCI formula has been developed at the leaf level [78,79]. Difficulties may arise when applying this vegetation index at crown level [80]. Generally, CCI and PRI are reliable indices for describing conifer phenology at the shoot level under laboratory conditions. However, NDVI, which is commonly used to describe the phenology of deciduous plants, is not suitable for measuring the phenology of *T. occidentalis*, *T. plicata*, and *P. orientalis* due to the saturation phenomenon [81,82].

In practice, the development of the method of remote diagnostics of phenological states of coniferous plants will make it possible to predict the effect of adverse climatic factors, diagnose stress states of plants, and plan management measures in coniferous plantations.

The results of the study have the following limitations—the study was conducted in laboratory conditions on the shoots of coniferous plants via proximal hyperspectral imaging. The established regularities can be used in remote sensing with certain assumptions.

A potential avenue for future research on the photosynthetic phenology of coniferous plants is the advancement of techniques for the remote diagnosis of the "Vegetation", "Dormancy", "Acclimatisation", and "Deacclimatisation" states. Additionally, it is crucial to promptly evaluate the level of frost tolerance of conifers during specific time periods. Currently, multispectral and hyperspectral data are used to determine the degree of damage to plants caused by negative temperatures [83,84] but not their frost tolerance—their ability to tolerate certain negative temperatures. The ability to solve this issue depends on the correlation between negative temperatures and the values of PRI and CCI. Additionally, during the frost period, highly frost-tolerant *T. occidentalis* and *T. plicata* exhibit significantly different levels of these VIs compared to weakly frost-tolerant *P. orientalis*.

5. Conclusions

The operational remote and proximal assessment of conifer plants' (plantation) condition throughout the annual cycle is important for predicting development, diagnosing stress conditions and planning agronomic measures. Photosynthetic phenology, using vegetation indices and spectral bands as metrics, can provide such opportunities. The study analyzed the time series of 81 vegetation index values and 125 spectral bands obtained from hyperspectral imagery for *T. occidentalis*, *T. plicata*, and *P. orientalis*. The time series of carotenoid sensitive vegetation indices (PRI, PRI_norm, PRI/CI2, and CCI) were found to have a more pronounced seasonal character than the time series of chlorophyll sensitive vegetation indices and spectral bands. Using these vegetation indices, "Vegetation" and "Dormancy" states were identified with 97.3% accuracy. The development of this research can be directed toward the development of methods for proximal and remote real-time assessments of frost tolerance in conifers.

Author Contributions: Conceptualization, P.A.D. and B.L.K.; data curation, B.L.K. and A.A.D.; formal analysis, A.A.D.; investigation, P.A.D. and A.A.D.; methodology, P.A.D.; project administration, P.A.D.; software, A.A.D.; writing—original draft, P.A.D. and B.L.K.; writing—review and editing, P.A.D. and B.L.K. All authors have read and agreed to the published version of the manuscript.

Funding: The project was supported by the Russian Science Foundation under grant No. 23-24-00390, https://rscf.ru/project/23-24-00390/ (accessed on 8 February 2024) and performed in Southern Federal University (Rostov-on-Don, Russian Federation).

Data Availability Statement: Data are contained within the article.

Conflicts of Interest: The authors declare no conflict of interest.

References

1. Vyse, K.; Pagter, M.; Zuther, E.; Hincha, D.K. Deacclimation after cold acclimation—A crucial, but widely neglected part of plant winter survival. *J. Exp. Bot.* **2019**, *70*, 4595–4604. [CrossRef]
2. North, M.; Workmaster, B.A.; Atucha, A. Effects of chill unit accumulation and temperature on woody plant deacclimation kinetics. *Physiol. Plant.* **2022**, *174*, e13717. [CrossRef]
3. Hu, X.-G.; Mao, J.-F.; El-Kassaby, Y.A.; Jia, K.-H.; Jiao, S.-Q.; Zhou, S.-S.; Li, Y.; Coops, N.C.; Wang, T. Local Adaptation and Response of *Platycladus orientalis* (L.) Franco Populations to Climate Change. *Forests* **2019**, *10*, 622. [CrossRef]
4. Wisniewski, M.; Bassett, C.; Gusta, L.V. An Overview of Cold Hardiness in Woody Plants: Seeing the Forest through the Trees. *HortScience* **2003**, *38*, 952–959. [CrossRef]
5. Strimbeck, G.R.; Schaberg, P.G.; Fossdal, C.G.; Schröder, W.P.; Kjellsen, T.D. Extreme low temperature tolerance in woody plants. *Front. Plant Sci.* **2015**, *6*, 884. [CrossRef]
6. Li, C.; Junttila, O.; Palva, E.T. Environmental regulation and physiological basis of freezing tolerance in woody plants. *Acta Physiol. Plant* **2004**, *26*, 213–222. [CrossRef]
7. Beck, E.H.; Heim, R.; Hansen, J. Plant resistance to cold stress: Mechanisms and environmental signals triggering frost hardening and dehardening. *J. Biosci.* **2004**, *29*, 449–459. [CrossRef] [PubMed]
8. Ensminger, I.; Sveshnikov, D.; Campbell, D.A.; Funk, C.; Jansson, S.; Lloyd, J.; Shibistova, O.; Öquist, G. Intermittent low temperatures constrain spring recovery of photosynthesis in boreal Scots pine forests. *Glob. Chang. Biol.* **2004**, *10*, 995–1008. [CrossRef]
9. Adams, W.W., III; Demmig-Adams, B. Carotenoid composition and down regulation of photosystem II in three conifer species during the winter. *Physiol. Plant.* **1994**, *92*, 451–458. [CrossRef]
10. Chang, C.Y.Y.; Bräutigam, K.; Hüner, N.P.A.; Ensminger, I. Champions of Winter Survival: Cold acclimation and Molecular Regulation of Cold Hardiness in Evergreen Conifers. *New Phytol.* **2020**, *229*, 675–691. [CrossRef] [PubMed]
11. Weiser, C.J. Cold Resistance and Injury in Woody Plants. *Science* **1970**, *169*, 1269–1278. [CrossRef]
12. Ferguson, J.; Moyer, M.M.; Mills, L.J.; Hoogenboom, G.; Keller, M. Modeling Dormant Bud Cold Hardiness and Budbreak in Twenty-Three Vitis Genotypes Reveals Variation by Region of Origin. *Am. J. Enol. Vitic.* **2013**, *65*, 59–71. [CrossRef]
13. Kovaleski, A.l.; Londo, J. Tempo of gene regulation in wild and cultivated Vitis species shows coordination between cold deacclimation and budbreak. *Plant Sci.* **2019**, *287*, 0168–9452. [CrossRef]
14. Salazar-Gutierrez, M.R.; Chaves, B.; Anothai, J.; Whiting, M.; Hoogenboom, G. Variation in cold hardiness of sweet cherry flower buds through different phenological stages. *Sci. Hortic.* **2014**, *172*, 161–167. [CrossRef]
15. Burr, K.; Hawkins, C.D.B.; L'Hirondelle, S.J.; Binder, W.D.; George, M.F.; Repo, T. Methods for Measuring Cold Hardiness of Conifers. *Tree Physiol.* **2001**, *1*, 369–401. [CrossRef]
16. Atucha Zamkova, A.A.; Steele, K.A.; Smith, A.R. Methods for Measuring Frost Tolerance of Conifers: A Systematic Map. *Forests* **2021**, *12*, 1094. [CrossRef]
17. Hawkins, C.; Lister, G. Invivo chlorophyll fluorescence as a possible indicator of the dormancy stage in Douglas-fir seedlings. *Can. J. For. Res.* **2011**, *15*, 607–612. [CrossRef]
18. Linkosalo, T.; Heikkinen, J.; Pulkkinen, P.; Mäkipää, R. Fluorescence measurements show stronger cold inhibition of photosynthetic light reactions in Scots pine compared to Norway spruce as well as during spring compared to autumn. *Front. Plant Sci.* **2014**, *5*, 264. [CrossRef]
19. Zhang, C.; Atherton, J.; Peñuelas, J.; Filella, I.; Kolari, P.; Aalto, J.; Ruhanen, H.; Bäck, J.; Porcar-Castell, A. Do all chlorophyll fluorescence emission wavelengths capture the spring recovery of photosynthesis in boreal evergreen foliage? *Plant Cell Environ.* **2019**, *42*, 3264–3279. [CrossRef] [PubMed]
20. Du, S.; Liu, L.; Liu, X.; Zhang, X.; Gao, X.; Wang, W. The Solar-Induced Chlorophyll Fluorescence Imaging Spectrometer (SIFIS) Onboard the First Terrestrial Ecosystem Carbon Inventory Satellite (TECIS-1): Specifications and Prospects. *Sensors* **2020**, *20*, 815. [CrossRef]
21. Lang, Q.; Zhiyong, Z.; Longsheng, C.; Hong, S.; Minzan, L.; Li, L.; Junyong, M. Detection of Chlorophyll Content in Maize Canopy from UAV Imagery. *IFAC-PapersOnLine* **2019**, *52*, 330–335. [CrossRef]

22. Noguera, M.; Aquino, A.; Ponce, J.M.; Cordeiro, A.; Silvestre, J.; Arias-Calderón, R.; Marcelo, M.; Jordão, P.; Andújar, J.M. Nutritional status assessment of olive crops by means of the analysis and modelling of multispectral images taken with UAVs. *Biosyst. Eng.* **2021**, *211*, 1–18. [CrossRef]
23. Perry, E.M.; Goodwin, I.; Cornwall, D. Remote Sensing Using Canopy and Leaf Reflectance for Estimating Nitrogen Status in Red-blush Pears. *HortScience* **2018**, *53*, 78–83. [CrossRef]
24. He, C.; Sun, J.; Chen, Y.; Wang, L.; Shi, S.; Qiu, F.; Wang, S.; Tagesson, T. A new vegetation index combination for leaf carotenoid-to-chlorophyll ratio: Minimizing the effect of their correlation. *Int. J. Digit. Earth* **2023**, *16*, 272–288. [CrossRef]
25. Haboudane, D.; Miller, J.R.; Tremblay, N.; Zarco-Tejada, P.J.; Dextraze, L. Integrated narrow-band vegetation indices for prediction of crop chlorophyll content for application to precision agriculture. *Remote Sens. Environ.* **2002**, *81*, 416–426. [CrossRef]
26. Antoniuk, V.; Zhang, X.; Andersen, M.N.; Kørup, K.; Manevski, K. Spatiotemporal Winter Wheat Water Status Assessment Improvement Using a Water Deficit Index Derived from an Unmanned Aerial System in the North China Plain. *Sensors* **2023**, *23*, 1903. [CrossRef]
27. Pôças, I.; Rodrigues, A.; Gonçalves, S.; Costa, P.M.; Gonçalves, I.; Pereira, L.S.; Cunha, M. Predicting Grapevine Water Status Based on Hyperspectral Reflectance Vegetation Indices. *Remote Sens.* **2015**, *7*, 16460–16479. [CrossRef]
28. Hansen, P.M.; Schjoerring, J.K. Reflectance measurement of canopy biomass and nitrogen status in wheat crops using normalized difference vegetation indices and partial least squares regression. *Remote Sens. Environ.* **2003**, *86*, 542–553. [CrossRef]
29. Lapaz Olveira, A.; Saínz Rozas, H.; Castro-Franco, M.; Carciochi, W.; Nieto, L.; Balzarini, M.; Ciampitti, I.; Reussi Calvo, N. Monitoring Corn Nitrogen Concentration from Radar (C-SAR), Optical, and Sensor Satellite Data Fusion. *Remote Sens.* **2023**, *15*, 824. [CrossRef]
30. Ma, H.; Cui, T.; Cao, L. Monitoring of Drought Stress in Chinese Forests Based on Satellite Solar-Induced Chlorophyll Fluorescence and Multi-Source Remote Sensing Indices. *Remote Sens.* **2023**, *15*, 879. [CrossRef]
31. Faqeerzada, M.A.; Park, E.; Kim, T.; Kim, M.S.; Baek, I.; Joshi, R.; Kim, J.; Cho, B.-K. Fluorescence Hyperspectral Imaging for Early Diagnosis of Heat-Stressed Ginseng Plants. *Appl. Sci.* **2023**, *13*, 31. [CrossRef]
32. Burnett, A.C.; Serbin, S.P.; Davidson, K.J.; Ely, K.S.; Rogers, A. Detection of the metabolic response to drought stress using hyperspectral reflectance. *J. Exp. Bot.* **2021**, *72*, 6474–6489. [CrossRef] [PubMed]
33. Bahe, M.M.; Murphy, R.L.; Russell, M.B.; Knight, J.F.; Johnson, G.R. Suitability of a single imager multispectral sensor for tree health analysis. *Urban For. Urban Green.* **2021**, *63*, 127187. [CrossRef]
34. Buitrago, M.F.; Groen, T.A.; Hecker, C.A.; Skidmore, A.K. Changes in thermal infrared spectra of plants caused by temperature and water stress. *ISPRS J. Photogramm. Remote Sens.* **2016**, *111*, 22–31. [CrossRef]
35. Xie, C.; Yang, C.; Moghimi, A. Detection of cold stressed maize seedlings for high throughput phenotyping using hyperspectral imagery. In Proceedings of the Hyperspectral Imaging Sensors: Innovative Applications and Sensor Standards 2017, Anaheim, CA, USA, 28 April 2017; Volume 10213, p. 1021305. [CrossRef]
36. Qiao, K.; Zhu, W.; Xie, Z.; Li, P. Estimating the Seasonal Dynamics of the Leaf Area Index Using Piecewise LAI-VI Relationships Based on Phenophases. *Remote Sens.* **2019**, *11*, 689. [CrossRef]
37. D'Odorico, P.; Besik, A.; Wong, C.Y.S.; Isabel, N.; Ensminger, I. High-throughput drone-based remote sensing reliably tracks phenology in thousands of conifer seedlings. *New Phytol.* **2020**, *226*, 1667–1681. [CrossRef]
38. Kowalski, K.; Senf, C.; Hostert, P.; Pflugmacher, D. Characterizing spring phenology of temperate broadleaf forests using Landsat and Sentinel-2 time series. *Int. J. Appl. Earth Obs. Geoinf.* **2020**, *92*, 102172. [CrossRef]
39. Wang, X.; Zhou, Y.; Wen, R.; Zhou, C.; Xu, L.; Xi, X. Mapping Spatiotemporal Changes in Vegetation Growth Peak and the Response to Climate and Spring Phenology over Northeast China. *Remote Sens.* **2020**, *12*, 3977. [CrossRef]
40. Venkatappa, M.; Anantsuksomsri, S.; Castillo, J.A.; Smith, B.; Sasaki, N. Mapping the Natural Distribution of Bamboo and Related Carbon Stocks in the Tropics Using Google Earth Engine, Phenological Behavior, Landsat 8, and Sentinel-2. *Remote Sens.* **2020**, *12*, 3109. [CrossRef]
41. Thapa, S.; Garcia Millan, V.E.; Eklundh, L. Assessing Forest Phenology: A Multi-Scale Comparison of Near-Surface (UAV, Spectral Reflectance Sensor, PhenoCam) and Satellite (MODIS, Sentinel-2) Remote Sensing. *Remote Sens.* **2021**, *13*, 1597. [CrossRef]
42. Liu, Z.; Jin, G.; Qi, Y. Estimate of Leaf Area Index in an Old-Growth Mixed Broadleaved-Korean Pine Forest in Northeastern China. *PLoS ONE* **2012**, *7*, e32155. [CrossRef]
43. D'Odorico, P.; Schönbeck, L.; Vitali, V.; Meusburger, K.; Schaub, M.; Ginzler, C.; Zweifel, R.; Velasco, V.M.E.; Gisler, J.; Gessler, A.; et al. Drone-based physiological index reveals long-term acclimation and drought stress responses in trees. *Plant Cell Environ.* **2021**, *44*, 3552–3570. [CrossRef]
44. Wong, C.Y.S.; D'Odorico, P.; Bhathena, Y.; Arain, M.A.; Ensminger, I. Carotenoid based vegetation indices for accurate monitoring of the phenology of photosynthesis at the leaf-scale in deciduous and evergreen trees. *Remote Sens. Environ.* **2019**, *233*, e111407. [CrossRef]
45. Gamon, J.A.; Huemmrich, K.F.; Wong, C.Y.S.; Ensminger, I.; Garrity, S.; Hollinger, D.Y.; Noormets, A.; Peñuelas, J. A remotely sensed pigment index reveals photosynthetic phenology in evergreen conifers. *Proc. Natl. Acad. Sci. USA* **2016**, *113*, 13087–13092. [CrossRef]
46. Springer, K.R.; Wang, R.; Gamon, J.A. Parallel Seasonal Patterns of Photosynthesis, Fluorescence, and Reflectance Indices in Boreal Trees. *Remote Sens.* **2017**, *9*, 691. [CrossRef]

47. Kincaid, J.A. Structure and dendroecology of *Thuja occidentalis* in disjunct stands south of its contiguous range in the central Appalachian Mountains. *USA For. Ecosyst.* **2016**, *3*, 25. [CrossRef]
48. Kozlovsky, B.L.; Ogorodnikova, T.K.; Kuropyatnikov, M.V.; Fedorinova, O.I. *Assortment of Woody Plants for Green Building in the Rostov Region*; Southern Federal University: Rostov-on-Don, Russia, 2009; p. 416, ISBN 978-5-9275-0674-3.
49. Li, G.; Du, S.; Wen, Z. Mapping the climatic suitable habitat of oriental arborvitae (*Platycladus orientalis*) for introduction and cultivation at a global scale. *Sci. Rep.* **2016**, *6*, 30009. [CrossRef] [PubMed]
50. Bareth, G.; Aasen, H.; Bendig, J.; Gnyp, M.L.; Bolten, A.; Jung, A.; Michels, R.; Soukkamäki, J. Low-weight and UAV-based hyperspectral full-frame cameras for monitoring crops: Spectral comparison with portable spectroradiometer measurements. *Photogramm. Fernerkund. Geoinf.* **2015**, *103*, 69–79. [CrossRef]
51. Aasen, H.; Burkart, A.; Bolten, A.; Bareth, G. Generating 3D hyperspectral information with lightweight UAV snapshot cameras for vegetation monitoring: From camera calibration to quality assurance. *JPRS* **2015**, *108*, 245–259. [CrossRef]
52. Dmitriev, P.A.; Kozlovsky, B.L.; Dmitrieva, A.A.; Varduni, T.V. Classification of invasive tree species based on the seasonal dynamics of the spectral characteristics of their leaves. *Earth Sci. Inform.* **2023**, *16*, 3729–3743. [CrossRef]
53. Tucker, C.J. Red and photographic infrared linear combinations for monitoring vegetation. *Remote Sens. Environ.* **1979**, *8*, 127–150. [CrossRef]
54. Gamon, J.A.; Gamon, J.A.; Peñuelas, J.; Field, C.B. A narrow-waveband spectral index that tracks diurnal changes in photosynthetic efficiency. *Remote Sens. Environ.* **1992**, *41*, 35–44. [CrossRef]
55. Dmitriev, P.A.; Kozlovsky, B.L.; Kupriushkin, D.P.; Dmitrieva, A.A.; Rajput, V.D.; Chokheli, V.A.; Tarik, E.P.; Kapralova, O.A.; Tokhtar, V.K.; Minkina, T.M.; et al. Assessment of Invasive and Weed Species by Hyperspectral Imagery in Agrocenoses Ecosystem. *Remote Sens.* **2022**, *14*, 2442. [CrossRef]
56. Blackburn, G.A. Hyperspectral remote sensing of plant pigments. *J. Exp. Bot.* **2007**, *58*, 855–867. [CrossRef] [PubMed]
57. Ustin, S.L.; Gitelson, A.A.; Jacquemoud, S.; Schaepman, M.; Asner, G.P.; Gamon, J.A.; Zarco-Tejada, P. Retrieval of foliar information about plant pigment systems from high resolution spectroscopy. *Remote Sens. Environ.* **2009**, *113*, S67–S77. [CrossRef]
58. Wong, C.Y.S. Tracking the phenology of photosynthesis using carotenoid-sensitive and near-infrared reflectance vegetation indices in a temperate evergreen and mixed deciduous forest. *New Phytol.* **2020**, *226*, 1682–1695. [CrossRef] [PubMed]
59. Lebrini, Y.; Boudhar, A.; Laamrani, A.; Htitiou, A.; Lionboui, H.; Salhi, A.; Chehbouni, A.; Benabdelouahab, T. Mapping and Characterization of Phenological Changes over Various Farming Systems in an Arid and Semi-Arid Region Using Multitemporal Moderate Spatial Resolution Data. *Remote Sens.* **2021**, *13*, 578. [CrossRef]
60. Wong, C.Y.S.; Gamon, J.A. The photochemical reflectance index provides an optical indicator of spring photosynthetic activation in evergreen conifers. *New Phytol.* **2015**, *206*, 196–208. [CrossRef]
61. Narmilan, A.; Gonzalez, F.; Salgadoe, A.S.A.; Kumarasiri, U.W.L.M.; Weerasinghe, H.A.S.; Kulasekara, B.R. Predicting Canopy Chlorophyll Content in Sugarcane Crops Using Machine Learning Algorithms and Spectral Vegetation Indices Derived from UAV Multispectral Imagery. *Remote Sens.* **2022**, *14*, 1140. [CrossRef]
62. Yue, J.; Feng, H.; Tian, Q.; Zhou, C. A robust spectral angle index for remotely assessing soybean canopy chlorophyll content in different growing stages. *Plant Methods* **2020**, *16*, 104. [CrossRef]
63. Sims, D.A.; Gamon, J.A. Relationships between leaf pigment content and spectral reflectance across a wide range of species, leaf structures and developmental stages. *Remote Sens. Environ.* **2002**, *81*, 337–354. [CrossRef]
64. Garrity, S.R.; Porcar-Castell, A.; Munné-Bosch, S.; Bäck, J.; Garbulsky, M.F.; Peñuelas, J. Disentangling the relationships between plant pigments and the Photochemical Reflectance Index reveals a new approach for remote estimation of carotenoid content. *Remote Sens. Environ.* **2011**, *115*, 628–635. [CrossRef]
65. Gamon, J.A.; Berry, J.A. Facultative and constitutive pigment effects on the Photochemical Reflectance Index (PRI) in sun and shade conifer needles. *Isr. J. Plant Sci.* **2012**, *60*, 85–95. [CrossRef]
66. Filella, I.; Porcar-Castell, A.; Munné-Bosch, S.; Bäck, J.; Garbulsky, M.F.; Peñuelas, J. PRI assessment of long-term changes in carotenoids/chlorophyll ratio and short-term changes in de-epoxidation state of the xanthophyll cycle. *Int. J. Remote Sens.* **2009**, *30*, 4443–4455. [CrossRef]
67. Asner, G.P.; Nepstad, D.; Cardinot, G.; Ray, D. Drought stress and carbon uptake in an Amazon forest measured with spaceborne imaging spectroscopy. *Proc. Natl. Acad. Sci. USA* **2004**, *101*, 6039–6044. [CrossRef]
68. Peguero-Pina, J.J.; Morales, F.; Flexas, J.; Gil-Pelegrín, E.; Moya, I. Photochemistry, remotely sensed physiological Reflectance index and deepoxidation state of the xanthophyll cycle in *Quercus coccifera* under intense drought. *Oecologia* **2008**, *156*, 1–11. [CrossRef]
69. Suarez, L.; Zarco-Tejada, P.J.; Sepulcre-Cantó, G.; Pérez-Priego, O.; Miller, J.R.; Jiménez-Muñoz, J.C.; Sobrino, J. Assessing canopy PRI for water stress detection with diurnal airborne imagery. *Remote Sens. Environ.* **2008**, *112*, 560–575. [CrossRef]
70. Damm, A.; Cogliati, S.; Colombo, R.; Fritsche, L.; Genangeli, A.; Genesio, L.; Hanus, J.; Peressotti, A.; Rademske, P.; Rascher, U.; et al. Response times of remote sensing measured sun-induced chlorophyll fluorescence, surface temperature and vegetation indices to evolving soil water limitation in a crop canopy. *Remote Sens. Environ.* **2022**, *273*, 112957. [CrossRef]
71. Kohzuma, K.; Tamaki, M.; Hikosaka, K. Corrected photochemical reflectance index (PRI) is an effective tool for detecting environmental stresses in agricultural crops under light conditions. *J. Plant Res.* **2021**, *134*, 683–694. [CrossRef]
72. Berni, J.A.J.; Zarco-Tejada, P.J.; Suarez, L.; Fereres, E. Thermal and Narrowband Multispectral Remote Sensing for Vegetation Monitoring from an Unmanned Aerial Vehicle. *IEEE Trans. Geosci. Remote Sens.* **2009**, *47*, 722–738. [CrossRef]

73. Zarco-Tejada, P.J.; González-Dugo, V.; Berni, J.A.J. Fluorescence, temperature and narrow-band indices acquired from a UAV platform for water stress detection using a micro-hyperspectral imager and a thermal camera. *Remote Sens. Environ.* **2012**, *117*, 322–337. [CrossRef]
74. Biriukova, K.; Pacheco-Labrador, J.; Migliavacca, M.; Mahecha, M.D.; Gonzalez-Cascon, R.; Martin, M.P.; Rossini, M. Performance of singular spectrum analysis in separating seasonal and fast physiological dynamics of solar-induced chlorophyll fluorescence and PRI optical signals. *J. Geophys. Res. Biogeosci.* **2021**, *126*, e2020JG006158. [CrossRef]
75. Wong, C.Y.S.; Gamon, J.A. Three causes of variation in the Photochemical Reflectance Index (PRI) in evergreen conifers. *New Phytol.* **2015**, *206*, 187–195. [CrossRef]
76. Pramsohler, M.; Neuner, G. Dehydration and osmotic adjustment in apple stem tissue during winter as it relates to the frost resistance of buds. *Tree Physiol.* **2013**, *33*, 807–816. [CrossRef]
77. Gamon, J.; Wang, R.; Russo, S.E. Contrasting photoprotective responses of forest trees revealed using PRI light responses sampled with airborne imaging spectrometry. *New Phytol.* **2023**, *238*, 1318–1332. [CrossRef]
78. Gitelson, A.A.; Zur, Y.; Chivkunova, O.; Merzlyak, M. Assessing carotenoid content in plant leaves with reflectance spectroscopy. *Photochem. Photobiol.* **2002**, *75*, 272–281. [CrossRef] [PubMed]
79. Gitelson, A.A.; Keydan, G.P.; Merzlyak, M.N. Three-band model for noninvasive estimation of chlorophyll, carotenoids, and anthocyanin contents in higher plant leaves. *Geophys. Res. Lett.* **2006**, *33*, L11402. [CrossRef]
80. Zarco-Tejada, P.J.; Guillén-Climent, M.L.; Hernández-Clemente, R.; Catalina, A.; González, M.R.; Martín, P. Estimating leaf carotenoid content in vineyards using high resolution hyperspectral imagery acquired from an unmanned aerial vehicle (UAV). *Agric. For. Meteorol.* **2013**, *171–172*, 281–294. [CrossRef]
81. Huang, S.; Tang, L.; Hupy, J.P.; Wang, Y.; Shao, G. A commentary review on the use of normalized difference vegetation index (NDVI) in the era of popular remote sensing. *J. For. Res.* **2021**, *32*, 1–6. [CrossRef]
82. Fawcett, D.; Bennie, J.; Anderson, K. Monitoring spring phenology of individual tree crowns using drone-acquired NDVI data. *Remote Sens. Ecol. Conserv.* **2020**, *7*, 227–244. [CrossRef]
83. Gabbrielli, M.; Corti, M.; Perfetto, M.; Fassa, V.; Bechini, L. Satellite-Based Frost Damage Detection in Support of Winter Cover Crops Management: A Case Study on White Mustard. *Agronomy* **2022**, *12*, 2025. [CrossRef]
84. Shammi, S.; Sohel, F.; Diepeveen, D.; Zander, S.; Jones, M.G.K. A survey of image-based computational learning techniques for frost detection in plants. *Inf. Process. Agric.* **2023**, *10*, 164–191. [CrossRef]